npj | Quantum Materials

www.nature.com/npjquantmats

ARTICLE OPEN

Check for updates

Spin-induced negative thermal expansion and spin–phonon coupling in van der Waals material $CrBr_3$

D. P. Kozlenko[1], O. N. Lis[1,2✉], S. E. Kichanov[1], E. V. Lukin[1], N. M. Belozerova[1] and B. N. Savenko[1]

The two-dimensional van der Waals (vdW) magnets retaining magnetic order in atomically thin limit demonstrate challenging physical phenomena and they are considered as prospective building blocks for construction of advanced spintronics and nanoelectronics devices. Here, we present experimental evidence for negative thermal expansion of lattice volume and vdW layers and strong spin–phonon coupling effects, caused by formation of the long-range ferromagnetic order in the vdW material $CrBr_3$. The neutron and X-ray diffraction measurements revealed anomalous temperature variation of lattice parameters and interatomic distances and angles in the vicinity of Curie temperature (T_C). A pronounced rise of the frequencies of the most of the observed vibrational modes and unusual reversal broadening of their full widths at half maximum below T_C was found from Raman spectroscopy measurements.

npj Quantum Materials (2021)6:19; https://doi.org/10.1038/s41535-021-00318-5

INTRODUCTION

Recent discovery of magnetism in the atomically thin two-dimensional (2D) van der Waals (vdW) materials has put them into focus of extensive scientific research due to importance of such materials for development of 2D spintronic and nanoelectronic devices as well as study of challenging physical phenomena like exotic quantum phases, topological spin excitations, etc.[1–6].

The family of cleavable layered semiconductors CrX_3 (X = Cl, Br, I) is of particular interest due to ferromagnetic intralayer coupling and comparable magnetic ordering temperatures in bulk and atomically thin forms[5,7,8]. The $CrBr_3$ crystallizes in the rhombohedral BiI_3 structure of $R\bar{3}$ symmetry and retains this structure at low temperatures. The CrI_3 and $CrCl_3$ crystallize in the monoclinic $AlCl_3$ structure of C2/m symmetry and undergo a structural phase transition to the rhombohedral $R\bar{3}$ structure below 210 and 240 K, respectively[8–10]. In the bulk form of $CrBr_3$ and CrI_3, both the intralayer and interlayer exchange couplings are ferromagnetic (FM), resulting in the formation of the FM ground state below T_C = 37 and 61 K. In the $CrCl_3$ the interlayer exchange coupling becomes antiferromagnetic (AFM), leading to appearance of the AFM ground state below $T_N = 17$ K[7–10]. Considering the 2D few-layered forms of these materials, in the case of $CrBr_3$ the intralayer and interlayer couplings remain ferromagnetic and the magnetic-ordering temperature in the monolayer limit decrease quite slightly to 27 K. In contrast, CrI_3 demonstrates a change of interlayer exchange coupling towards antiferromagnetic one and the magnetic ordering temperature is reduced more significantly to 45 K in the monolayer limit. In $CrCl_3$, the interlayer coupling retains antiferromagnetic nature and the magnetic-ordering temperature remains about the same, $T_N = 16$ K in the two-layer limit[7].

In the few-layer forms of CrX_3 and heterostructures containing these materials a number of emerging phenomena, including electric field and stacking-dependent control of magnetism, giant tunneling magnetoresistance, giant nonreciprocal second harmonics generation, magnetic proximity effect, important for development of broad range spintronic devices, was observed[11–17]. These phenomena arise from a complex interplay of various degrees of freedom associated with the charge carriers and atomic layers. One of the factors, playing important role in such interplay, is the spin–lattice coupling. A pronounced spin–lattice coupling was recently found in the vdW material $Cr_2Ge_2Te_6$[18]. In bulk $CrCl_3$, an anomaly in magnetic susceptibility at the low-temperature structural phase transition was observed, pointing to a presence of spin–lattice coupling[10].

A perfect model system to search for emergent physical phenomena, associated with the spin–lattice coupling in the CrX_3 family, is $CrBr_3$ due to absence of structural phase transitions at low temperatures and similarity of magnetic order in bulk and few-layer forms. Using a combination of the X-ray, neutron powder diffraction, and Raman spectroscopy, we revealed a negative thermal volume expansion (NTE) phenomenon in $CrBr_3$ below the Curie temperature with a coefficient $\alpha_V = -1.9 \times 10^{-5}$ K^{-1}. The relevant coefficient, characterizing linear thermal expansion of the 2D vdW layers in $CrBr_3$, $\alpha_l = -1.6 \times 10^{-5}$ K^{-1}, is also negative and comparable by the order of magnitude with one of graphene at low temperatures. The observed anomalies in the temperature behavior of lattice parameters, interatomic distances and angles as well as vibrational modes frequencies and linewidths provide clear evidence for a strong coupling between spin and lattice degrees of freedom in ferromagnetic vdW magnets of CrX_3 family and related materials.

RESULTS AND DISCUSSION

Neutron and X-ray diffraction

The neutron diffraction patterns of $CrBr_3$ measured at selected temperatures are shown in Fig. 1a. They are consistent with the rhombohedral crystal structure of $R\bar{3}$ symmetry in the whole studied temperature range of 6–300 K. In this structure (Fig. 1b), Cr^{3+} ions arrange in the honeycomb magnetic lattice and they are surrounded by edge-sharing octahedra formed by Br^- ions. The Br–Cr–Br layers are stacked along the *c*-axis and bonded by the vdW forces. The obtained lattice parameters (in hexagonal setting) at ambient conditions, $a = 6.3019(2)$ and $c = 18.332(1)$ Å are consistent with previous studies[8,19].

[1]Frank Laboratory of Neutron Physics, JINR, Dubna, Moscow Reg., Russian Federation. [2]Kazan Federal University, Kazan, Russian Federation. ✉email: lisa_9477@mail.ru

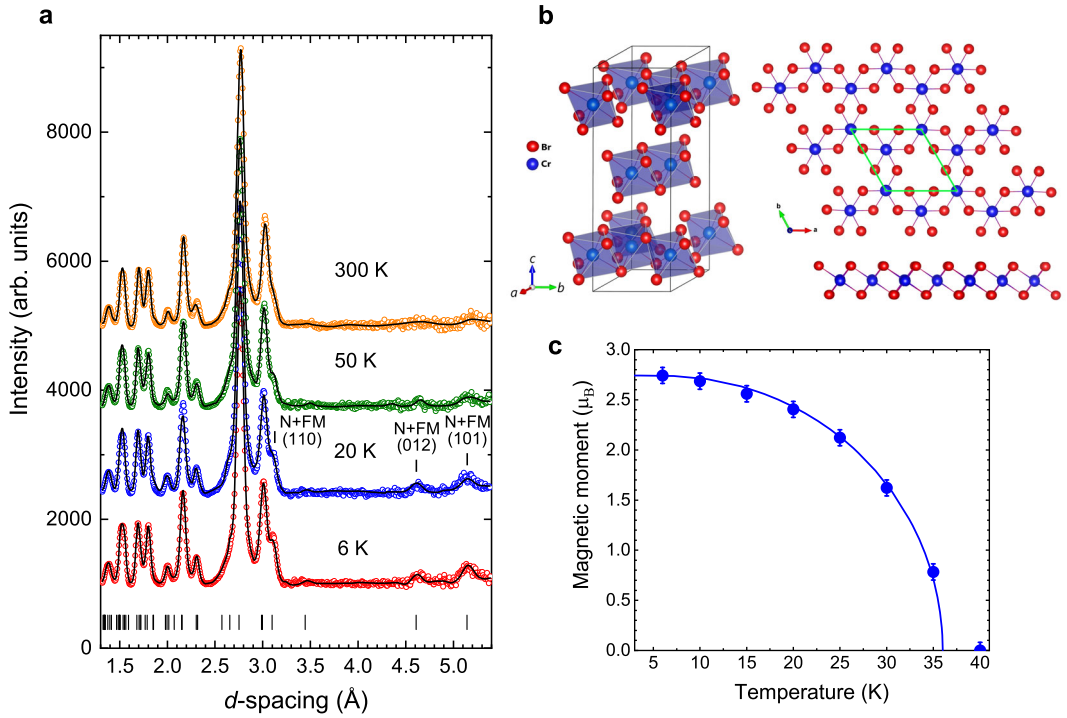

Fig. 1 Neutron diffraction patterns and crystal structure of $CrBr_3$. a Neutron diffraction patterns of $CrBr_3$ measured at selected temperatures and refined by the Rietveld method. The experimental points and calculated profiles are shown. The ticks below represent the calculated positions of the structural peaks of rhombohedral phase of $CrBr_3$ for selected temperatures. The characteristic peaks with magnetic scattering contribution superimposed on nuclear scattering contribution are marked as "N+FM" and their (*hkl*) indexes are given. **b** The rhombohedral structure of van der Waals crystal $CrBr_3$ of $R\bar{3}$ symmetry. The unit cell (**a**), top view (**b**) and side view of a single layer (**c**) are shown. **c** The Cr^{3+}-ordered magnetic moment as function of temperature, fitted by the expression (1).

On cooling below 35 K, an appearance of additional magnetic scattering contribution to intensities of the peaks (110), (012), and (101) was detected (Fig. 1a), evidencing formation of the FM ground state. The temperature dependence of the Cr^{3+}-ordered magnetic moments (Fig. 1c) evaluated from the neutron diffraction data, can be well fitted in the framework of the molecular field approach

$$\frac{M}{M_0} = B_s\left(\frac{3S}{S+1}\frac{M}{M_0}\frac{T_C}{T}\right), \quad (1)$$

where B_s is the Brillouin function, S is the spin of the system ($S = 3/2$) and M_0 is the ordered magnetic moment at $T = 0$. The calculated values of the magnetic ordering temperature $T_C = 36$ (2) K and $M_0 = 2.74(8)$ μ_B were obtained. The M_0 value is consistent with one of 2.83 μ_B, determined from the polarized neutron diffraction study[20]. The ordered magnetic moments are oriented along the *c*-axis, in accordance with the easy spin axis direction[7,21].

The temperature dependences of the lattice parameters and volume normalized to the ambient temperature values obtained from neutron and X-ray diffraction measurements are shown in Fig. 2. The thermal expansion of $CrBr_3$ lattice is strongly anisotropic with the pronounced variation of the *c* lattice parameter. The temperature dependence of the *a* lattice parameter demonstrates anomalous behavior. Its thermal expansion changes from conventional positive character in the temperature range above T_C to unexpected negative character below T_C. This also results in negative thermal expansion of the unit cell volume for $T < T_C$ (Fig. 2). The average volume thermal expansion coefficients ($\alpha_V = (1/V)(dV/dT)$) are $\alpha_V = 3.6 \times 10^{-5}\,K^{-1}$ for $T > T_C$ and $\alpha_V = -1.9 \times 10^{-5}\,K^{-1}$ for $T < T_C$, respectively. The latter value is about twice larger in comparison with one for the frustrated antiferromagnetic spinel material $ZnCr_2Se_4$, $\alpha_V = -1.08 \times 10^{-5}\,K^{-1}$ for 21–40 K[22].

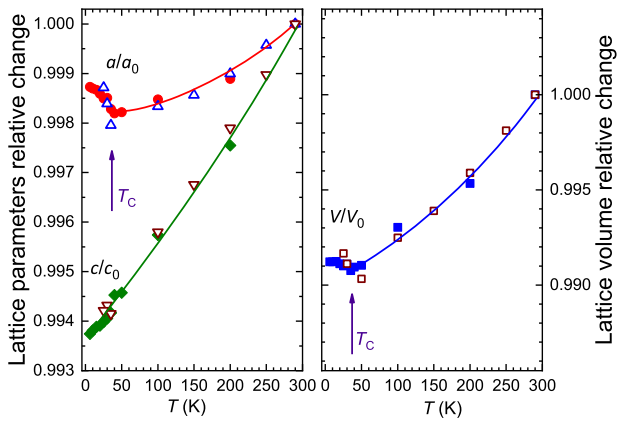

Fig. 2 The temperature dependences of the lattice parameters of $CrBr_3$. The temperature dependences of the lattice parameters and volume obtained from neutron (solid symbols) and X-ray diffraction (open symbols) measurements and normalized to the ambient temperature values. The lines are guides to eyes only.

It should be noted that information about thermal expansion behavior is of special importance for fabrication of heterostructures involving vdW materials and their practical applications. The difference in thermal expansion of neighboring layers may result in appearance of strains, significantly affecting the physical properties. The corresponding average linear thermal expansion coefficients of the *a* lattice parameter ($\alpha_l = (1/a)(da/dT)$), characterizing thermal expansion of the 2D vdW layers in $CrBr_3$, are $\alpha_l = 0.7 \times 10^{-5}\,K^{-1}$ for $T > T_C$ and $\alpha_l = -1.6 \times 10^{-5}\,K^{-1}$ for $T < T_C$, respectively. The graphene, one of the most popular 2D materials for design of heterostructures, also demonstrates negative thermal expansion over a wide range of temperatures with $\alpha_l =$

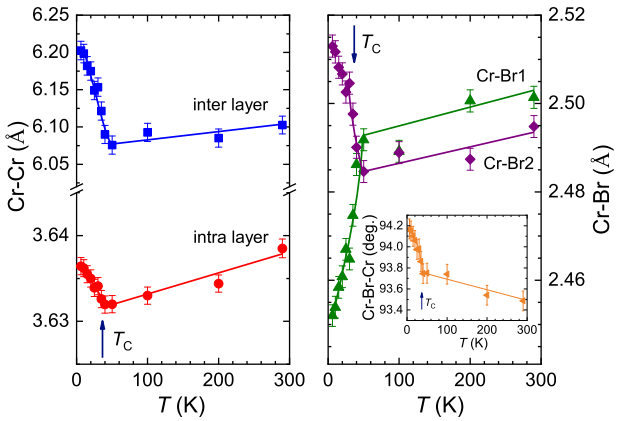

Fig. 3 The evolution of interatomic distances and angles as a function of temperature. The temperature dependences of the interatomic distances and angles in $CrBr_3$. The lines are guides to eyes only.

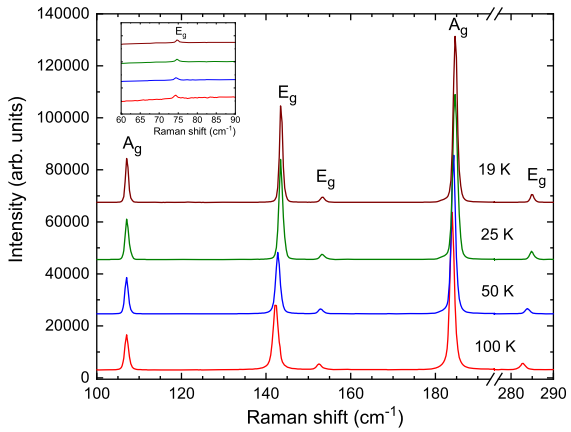

Fig. 4 The Raman spectra of $CrBr_3$. The Raman spectra, measured at selected temperatures. The inset shows enlarged sections of the spectra in the Raman shift region of 60–90 cm^{-1}.

-1.5×10^{-5} K^{-1} for $T = 200$ K and evaluated average $\alpha_l \approx -0.5 \times 10^{-5}$ K^{-1} for $T < 50$ K[23], comparable by an order of magnitude with those of vdW layers of $CrBr_3$.

The interatomic intralayer and interlayer Cr–Cr distances decrease slightly on cooling in the temperature range above T_C and they also demonstrate opposite increasing trend for $T < T_C$ (Fig. 3). In the bromium octahedral units forming inside the vdW layers around chromium ions (Fig. 1b), there are two non-equivalent types of interatomic distances, three pairs of Cr–Br1 and three pairs of Cr–Br2 ones. Both distances have comparable values of 2.501(2) and 2.495(2) Å at ambient temperatures and they are weakly reduced on cooling downwards the Curie temperature. Below T_C, a pronounced anisotropic distortion of the octahedral units occurs, resulting in reduction of the Cr–Br1 distances to 2.452(2) Å and enlargement of the Cr–Br2 distances to 2.513(2) Å at $T = 6$ K, respectively (Fig. 3). The temperature behavior of the Cr–Br–Cr interatomic angles, mediating ferromagnetic superexchange interactions, demonstrates growing trend on cooling in the temperature range above T_C and anomaly in the vicinity of T_C, caused by rapidly enhanced temperature variation rate. The anomalous behavior of the thermal expansion in the plane, perpendicular to the magnetic easy axis c, interatomic distances and angles in the vicinity of T_C are caused by a complex interplay between the spin and lattice degrees of freedom in $CrBr_3$.

Raman spectroscopy

In the Raman spectra of $CrBr_3$, measured at selected temperatures, the six lines were observed (Fig. 4). The factor group analysis predicts eight Raman active modes, $\Gamma_{ram} = (4A_g + 4E_g)$ for the rhombohedral $R\bar{3}$ lattice symmetry (corresponding point group C_{3i}) of this material[24,25]. The detected lines were tentatively assigned as 74.0 cm^{-1} (E_g), 106.3 cm^{-1} (A_g), 141.3 cm^{-1} (E_g), 150.4 cm^{-1} (E_g), 182.4 cm^{-1} (A_g), 278.0 cm^{-1} (E_g) phonon modes, according to refs. [24–26].

In the paramagnetic region, the frequencies of observed phonon modes (Fig. 5) demonstrate increasing trend with a temperature lowering, while full-width at half-maximum (FWHM) of relevant phonon peaks decreases. In the anharmonic approach, the corresponding temperature dependences can be described as

$$\nu(T) = \nu_0 + A_1(1 + 2n_B(\nu_0/2)) + A_2[1 + 3n_B(\nu_0/3) + 3(n_B(\nu_0/3))^2],$$
$$\mathrm{FWHM}(T) = \mathrm{FWHM}_0 + B_1(1 + 2n_B(\nu_0/2)) + B_2[1 + 3n_B(\nu_0/3) + 3(n_B(\nu_0/3))^2], \quad (2)$$

where ν_0 is the harmonic phonon frequency, FWHM_0 is the phonon broadening induced by disorder, n_B is the thermal

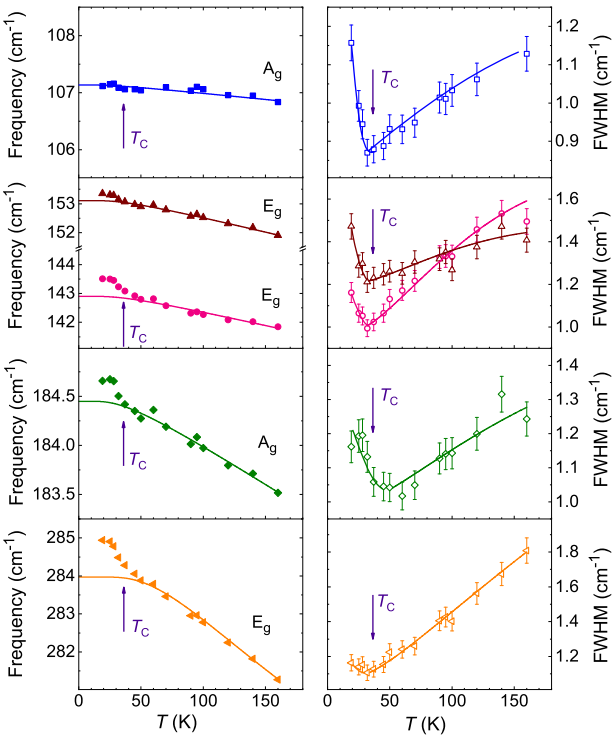

Fig. 5 The temperature dependences of selected Raman peak frequencies and full-width at half-maximum (FWHM). The solid lines represent the fitting results in the anharmonic approach as described in the text.

population Bose factor, A_1 (B_1) and A_2(B_2) are the coefficients, described contributions of cubic and quartic anharmonic terms[18,27].

Below T_C, a rapid increase of the phonon frequencies in the energy range above 150 cm^{-1} occurs compared to thermal behavior expected within the anharmonic approach. The FWHM of all the observed phonon modes reach minimum in the vicinity of T_C and demonstrate anomalous reversal broadening in the $T < T_C$ range (Fig. 5). Both effects reveal a presence of the strong spin–phonon coupling in $CrBr_3$. The spin–phonon coupling is associated with the modification of the magnetic exchange interactions caused by the ionic motions, and the relevant

Table 1. The spin–phonon coupling constants in $CrBr_3$ at $T = 19$ K.

Mode	ν (cm^{-1})	ν_0 (cm^{-1})	λ (cm^{-1})
E_g	143.5 (2)	142.9 (2)	0.27 (1)
E_g	153.4 (2)	153.1 (2)	0.13 (1)
A_g	184.7 (2)	184.4 (2)	0.13 (1)
E_g	284.9 (3)	284.0 (3)	0.40 (2)

phonon frequency shifts can be expressed as

$$\nu(T) = \nu_0 + \lambda\langle S_i \cdot S_j \rangle, \quad (3)$$

where ν_0 is the frequency in the absence of spin–phonon interactions, λ is the spin–phonon coupling constant, and $\langle S_iS_j\rangle$ is the spin–spin correlation function of the neighboring spins[28]. The value of the spin–phonon coupling constant for a given phonon mode can be evaluated to the first order of magnitude as $I \sim \sum_{i,\alpha}\left(\frac{\partial J}{\partial u_{i,\alpha}}\right)u_{i,\alpha}$, where J is the nearest-neighbor exchange integral, $u_{i,\alpha}$ is the ionic displacement components $\alpha = (x,y,z)$ taken for atoms i contributing to the considered mode[29,30]. The evaluated spin–phonon coupling constants for various Raman modes, calculated using the value of $S = 3/2$ for Cr^{3+} spins, are presented in the Table 1. The largest values of $\lambda = 0.27$ and $0.40\,cm^{-1}$ are found for the E_g modes with frequencies of 143.5 and $284.9\,cm^{-1}$, respectively. According to the theoretical calculations performed for the FM phase of relevant CrI_3 compound[26], these phonon modes involve vibrations of the magnetic chromium ions, providing more pronounced coupling effects. In particular, the E_g mode at $284.9\,cm^{-1}$ involves out-of-phase vibrations of two in-plane Cr atoms only, resulting in enhanced sensitivity to the onset of magnetic order. The λ coefficients are comparable with those reported for another vdW ferromagnet $Cr_2Ge_2Te_6$[18], although about an order of magnitude less compared to antiferromagnetic chromium spinels[31].

The present results demonstrate a strong and complex interplay between spin and lattice degrees of freedom in the vdW material $CrBr_3$. Below the Curie temperature a pronounced negative thermal volume expansion and linear expansion of the 2D vdW layers in $CrBr_3$ with the coefficients $\alpha_V = -1.9 \times 10^{-5}\,K^{-1}$ and $\alpha_l = -1.6 \times 10^{-5}\,K^{-1}$ are revealed. The latter value is comparable by the order of magnitude with one of graphene at low temperatures. These effects are also accompanied by anomalous thermal variation of interatomic distances and angles. The associated spin–phonon coupling effects provoke extra rise of the most of the observed vibrational modes frequencies and reversal broadening of their FWHM values, particularly pronounced for the modes involving vibrations of the magnetic chromium ions.

METHODS

Samples

The single crystalline $CrBr_3$ samples were supplied by HQ Graphene.

Neutron diffraction

The neutron diffraction measurements with the powdered samples were performed in the temperature range 6–300 K using the DN-6 diffractometer at the IBR-2 high flux pulsed reactor with the CCR-based refrigerator[32]. The diffraction patterns were collected at the scattering angle of 90° with the resolution of $\Delta d/d = 0.022$. The sample volume was about $5\,mm^3$. The neutron diffraction patterns were analyzed by the Rietveld method using the Fullprof program[33].

X-ray diffraction

The X-ray powder diffraction measurements were performed in the temperature range 15–300 K using the Malvern PANalytical Empyrean diffractometer with the Cu K_α radiation, $\lambda = 1.541$ Å, and the CCR-based refrigerator. The X-ray diffraction patterns were also analyzed by the Rietveld method using the Fullprof program[33].

Raman spectroscopy

The Raman spectra with the single crystalline $CrBr_3$ samples were collected using a LabRAM HR Evolution spectrometer (Horiba, France) with a wavelength excitation of 632.8 nm emitted from He–Ne laser, 1800 grating, confocal hole of 200 μm, and ×20 objective. The low-temperature Raman measurements were carried out using low vibration helium refrigerator (Advanced Research Systems, USA) in temperature range 19–300 K.

DATA AVAILABILITY

The data that support the findings of this study are available from the corresponding author on a reasonable request.

Received: 9 September 2020; Accepted: 26 January 2021;
Published online: 02 March 2021

REFERENCES

1. Gong, C et al. Discovery of intrinsic ferromagnetism in two-dimensional van der Waals crystals. *Nature* **546**, 265–269 (2017).
2. Burch, K. S., Mandrus, D. & Park, J.-G. Magnetism in two-dimensional van der Waals materials. *Nature* **563**, 47–52 (2018).
3. Gibertini, M., Koperski, M., Morpurgo, A. F. & Novoselov, K. S. Magnetic 2D materials and heterostructures. *Nat. Nanotechnol.* **14**, 408–419 (2019).
4. Zhang, W., Wong, P. K. J., Zhu, R. & Wee, A. T. S. Van der Waals magnets: wonder building blocks for two-dimensional spintronics? *InfoMat* **1**, 479–495 (2019).
5. Huang, B. et al. Layer-dependent ferromagnetism in a van der Waals crystal down to the monolayer limit. *Nature* **546**, 270–273 (2017).
6. Ding, B. et al. Observation of magnetic skyrmion bubbles in a van der Waals ferromagnet Fe_3GeTe_2. *Nano Lett.* **20**, 868–873 (2020).
7. Kim, H. H. et al. Evolution of interlayer and intralayer magnetism in three atomically thin chromium trihalides. *Proc. Natl Acad. Sci. USA* **116**, 11131–11136 (2019).
8. Samuelsen, E. J., Silberglitt, R., Shirane, G. & Remeika, J. P. Spin waves in ferromagnetic $CrBr_3$ studied by inelastic neutron scattering. *Phys. Rev. B* **3**, 157–166 (1971).
9. McGuire, M. A., Dixit, H., Cooper, V. R. & Sales, B. S. Coupling of crystal structure and magnetism in the layered, ferromagnetic insulator CrI_3. *Chem. Mater.* **27**, 612–620 (2015).
10. McGuire, M. A. et al. Magnetic behavior and spin–lattice coupling in cleavable van der Waals layered $CrCl_3$ crystals. *Phys. Rev. Mater.* **1**, 014001 (2017).
11. Huang, B. et al. Electrical control of 2D magnetism in bilayer CrI_3. *Nat. Nanotechnol.* **13**, 544–548 (2018).
12. Jiang, S., Shan, J. & Mak, K. F. Electric-field switching of two-dimensional van der Waals magnets. *Nat. Mater.* **17**, 406–410 (2018).
13. Chen, W. et al. Direct observation of van der Waals stacking-dependent interlayer magnetism. *Science* **366**, 983–987 (2019).
14. Kim, H. H. et al. One million percent tunnel magnetoresistance in a magnetic van der Waals heterostructure. *Nano Lett.* **18**, 4885–4890 (2018).
15. Sun, Z. et al. Giant nonreciprocal second-harmonic generation from antiferromagnetic bilayer CrI_3. *Nature* **572**, 497–501 (2019).
16. Tang, C., Zhang, Z., Lai, S., Tan, Q. & Gao, W.-B. Magnetic proximity effect in graphene/$CrBr_3$ van der Waals heterostructures. *Adv. Mater.* **32**, 1908498 (2020).
17. Karpiak, B. et al. Magnetic proximity in a van der Waals heterostructure of magnetic insulator and graphene. *2D Materials* **7**, 015026 (2020).
18. Tian, Y. et al. Magneto-elastic coupling in a potential ferromagnetic 2D atomic crystal. *2D Materials* **3**, 025035 (2016).
19. Zhang, W.-B., Qu, Q., Zhu, P. & Lam, C.-H. Robust intrinsic ferromagnetism and half semiconductivity in stable two-dimensional single-layer chromium trihalides. *J. Mater. Chem. C* **3**, 12457–12468 (2015).
20. Radhakrishna, P. & Brown, P. J. Polarized neutron-diffraction study of spin-density distribution in chromium tribromide. *Phys. Rev. B* **36**, 8765–8771 (1987).
21. Tsubokawa, I. On the magnetic properties of a $CrBr_3$ single crystal. *J. Phys. Soc. Jpn.* **15**, 1664–1668 (1960).
22. Chen, J., Hu, L., Deng, J. & Xing, X. Negative thermal expansion in functional materials: controllable thermal expansion by chemical modifications. *Chem. Soc. Rev.* **44**, 3522–3567 (2015).
23. Yoon, D., Son, Y.-W. & Cheong, H. Negative thermal expansion coefficient of graphene measured by Raman spectroscopy. *Nano Lett.* **11**, 3227–3231 (2011).

24. Bermudez, V. M. Unit-cell vibrational spectra of chromium trichoride and chromium tribromide. *Solid State Commun.* **19**, 693–697 (1976).
25. Larson, D. T. & Kaxiras, E. Raman spectrum of CrI_3: an ab initio study. *Phys. Rev. B* **98**, 085406 (2018).
26. Webster, L., Liang, L. & Yan, J.-A. Distinct spin–lattice and spin–phonon interactions in monolayer magnetic CrI_3. *Phys. Chem. Chem. Phys.* **20**, 23546–23555 (2018).
27. Balkanski, M., Wallis, R. F. & Haro, E. Anharmonic effects in light scattering due to optical phonons in silicon. *Phys. Rev. B* **28**, 1928–1934 (1983).
28. Lockwood, D. J. & Cottam, M. G. The spin–phonon interaction in FeF_2 and MnF_2 studied by Raman spectroscopy. *J. Appl. Phys.* **64**, 5876–5878 (1988).
29. Fleury, P. A. & Loudon, R. Scattering of light by one- and two-magnon excitations. *Phys. Rev.* **166**, 514–530 (1968).
30. Werner, R., Gros, C. & Braden, M. Microscopic spin-phonon coupling constants in $CuGeO_3$. *Phys. Rev. B* **59**, 14356–14366 (1999).
31. Rudolf, T. et al. Spin–phonon coupling in antiferromagnetic chromium spinels. *New J. Phys.* **9**, 76 (2007).
32. Kozlenko, D., Kichanov, S., Lukin, E. & Savenko, B. The DN-6 neutron diffractometer for high-pressure research at half a megabar scale. *Crystals* **8**, 331 (2018).
33. Rodríguez-Carvajal, J. Recent advances in magnetic structure determination by neutron powder diffraction. *Physica B* **192**, 55–69 (1993).

ACKNOWLEDGEMENTS

The authors acknowledge technical assistance of Dr. V.A. Turchenko (JINR) with the X-ray diffraction measurements.

AUTHOR CONTRIBUTIONS

D.P.K. initiated the research. D.P.K., S.E.K., E.V.L. and B.N.S. performed the neutron diffraction experiments and data analysis. O.N.L. and E.V.L. performed the X-ray diffraction experiments and data analysis. O.N.L. and N.M.B. performed the Raman spectroscopy experiments and data analysis. D.P.K. and O.N.L. prepared first draft of the manuscript and all the co-authors contribute to the final version of the manuscript.

COMPETING INTERESTS

The authors declare no competing interests.

ADDITIONAL INFORMATION

Correspondence and requests for materials should be addressed to O.N.L.

Reprints and permission information is available at http://www.nature.com/reprints

Publisher's note Springer Nature remains neutral with regard to jurisdictional claims in published maps and institutional affiliations.